Chronic Administration of the *N*-Methyl-D-Aspartate Receptor Antagonist Ketamine Improves Rett Syndrome Phenotype

Supplementary Information

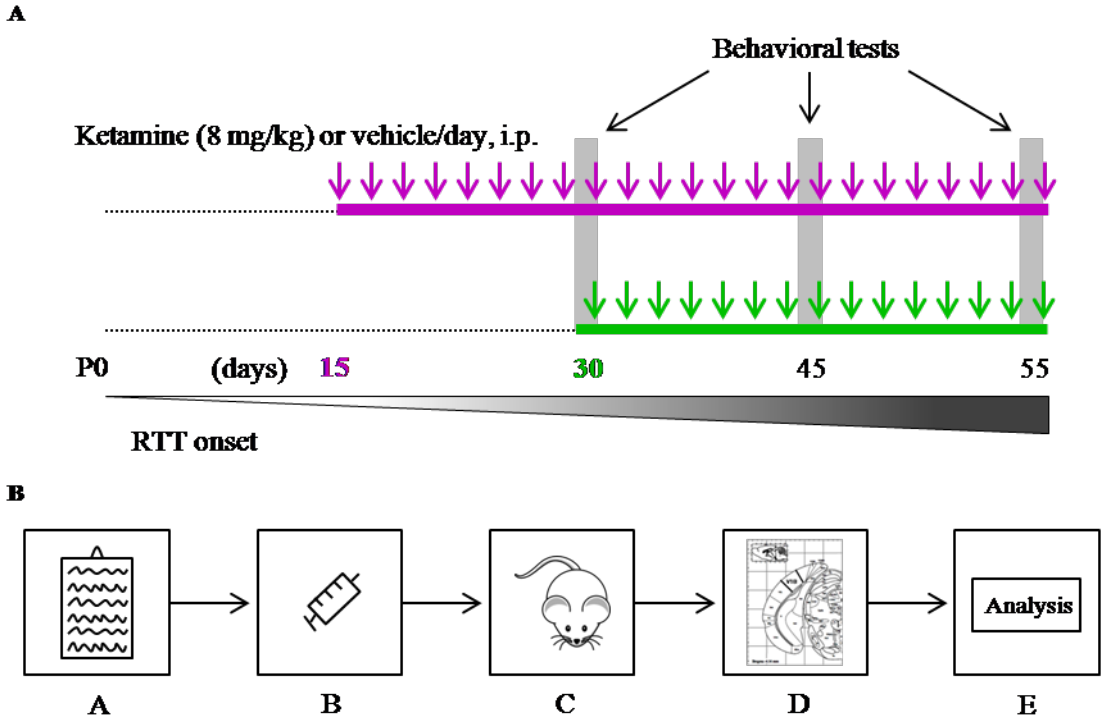

Figure S1. Randomized pre-clinical experimental paradigm. (A) *Mecp2* WT and KO mice were administered ketamine (8 mg/kg) or vehicle daily starting from P15 (magenta, top line) or from P30 (green, bottom line). A tailored battery of behavioral tests was performed every 15 days (gray columns) starting from P30. Arrows indicate the duration of the treatment. **(B)** Schematic representation of the study design. Random allocation of *Mecp2* WT and KO mice (A), daily ketamine administration (B), behavioral analysis (C), functional and anatomical study (D) and experimental analysis (E) were performed by a different set of researchers.

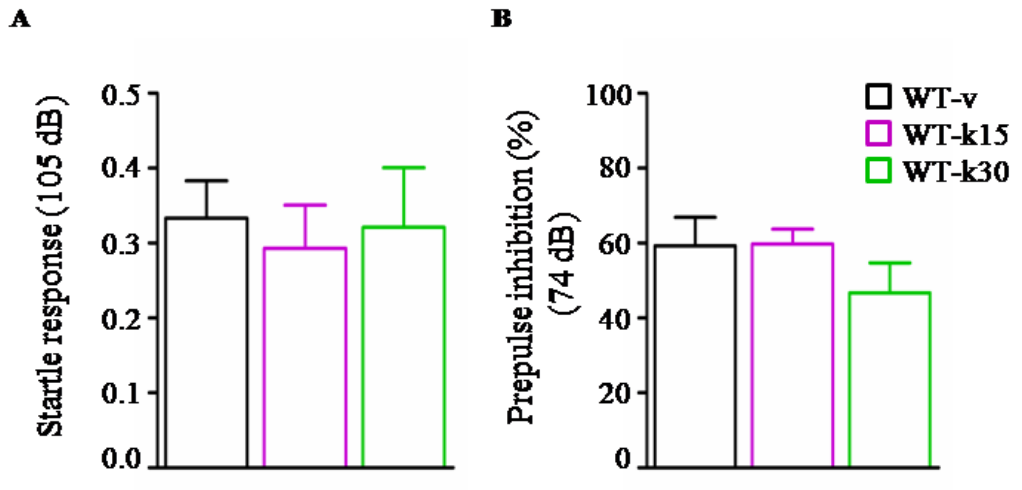

Figure S2. Prolonged ketamine treatment does not altered prepulse inhibition behavior. No modification in acoustic startle **(A)** and prepulse inhibition **(B)** responses were observed in adult WT mice treated daily with 8 mg/kg of ketamine starting either at P15 (WT-k15) or at P30 (WT-k30). (Kruskal-Wallis, $p \geq 0.05$. WT-v, $n = 5$; WT-k15, $n = 9$; WT-k30, $n = 7$ mice). Data are expressed as mean ± SEM.

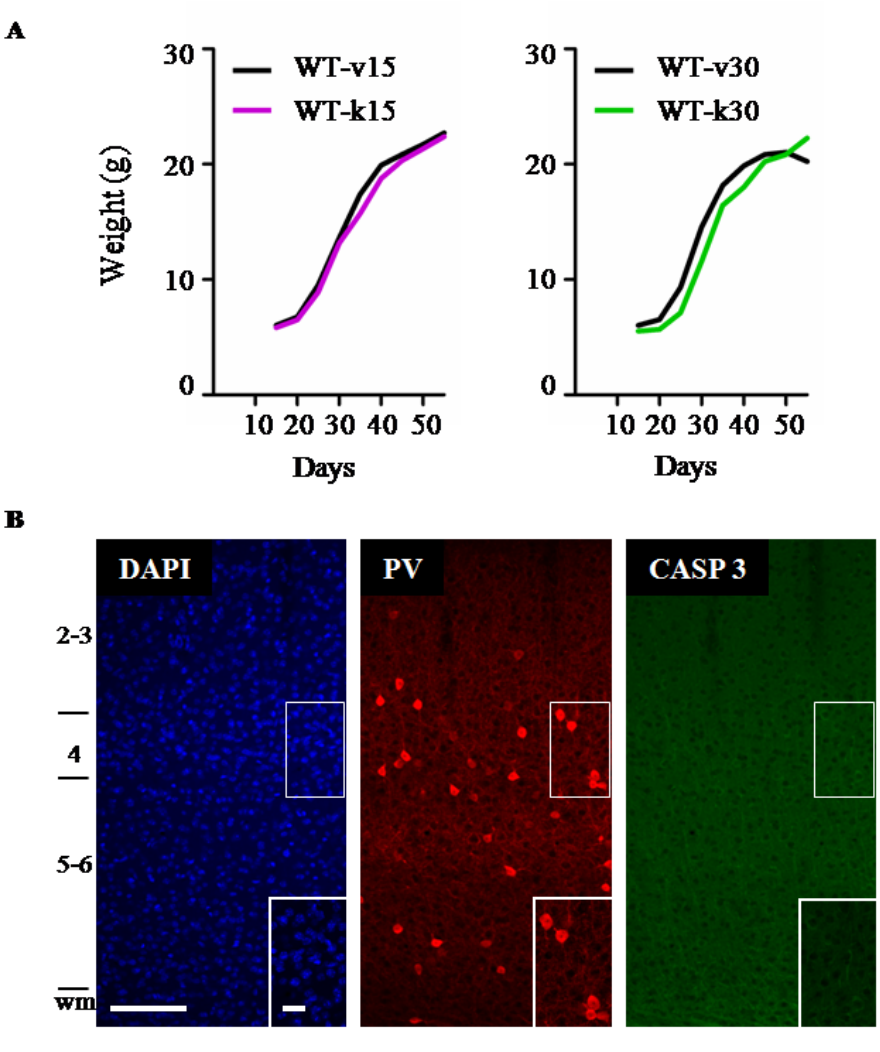

C

NeuN density	WT-v	KO-v15	KO-k15	KO-v30	KO-k30
μm^2	23.1 ± 0.7	23.0 ± 0.4	24.5 ± 0.8	23.7 ± 0.2	22.28 ± 0.6
μm^3	3.5 ± 0.3	3.5 ± 0.1	3.8 ± 0.2	4.0 ± 0.2	3.2 ± 0.2

Figure S3. Prolonged ketamine treatment in WT animals does not cause detrimental outcomes. (A) Chronic ketamine treatment did not cause weight loss in WT mice (Kolmogorov-Smirnov, $p \geq 0.05$. WT-v15, $n = 6$; WT-k15, $n = 13$; WT-v30, $n = 5$; WT-k30, $n = 10$). **(B)** Representative confocal images showing DAPI (blue), parvalbumin (PV, red) and Caspase 3 (CASP 3, green) in *Mecp2*-null mice treated chronically with ketamine starting from P15. Notably, no CASP 3-positive cells were present throughout the visual cortex. (Scale bar 100 mm low magnification, 20 mm high magnification). **(C)** No differences in NeuN cell density were detected in chronically treated *Mecp2*-null mice (Kruskal-Wallis, $p \geq 0.05$).

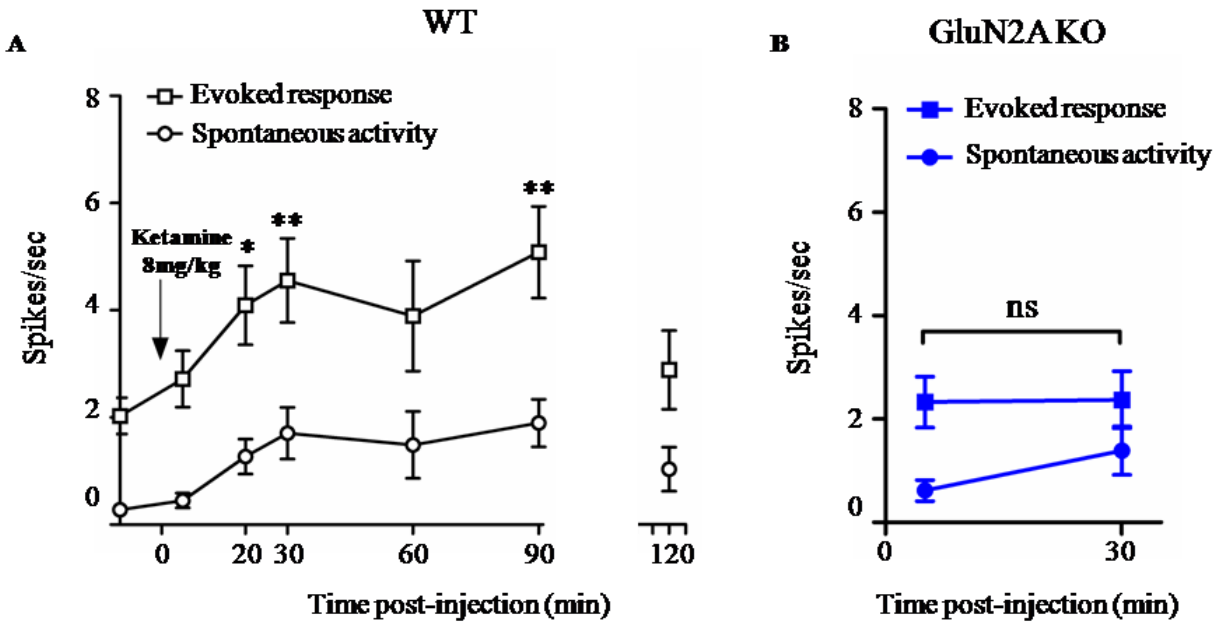

Figure S4. Ketamine increases pyramidal cells activity by acting on NMDA-GluN2A receptors. (A) An acute ketamine (i.p., 8 mg/kg) administration increased the average of maximal evoked response and spontaneous activity in pyramidal cells in V1 (Friedman test, *p < 0.05, **p < 0.01, Dunn's post test. n = 38 from 4 mice). **(B)** In GluN2A KO mice no significant increase was revealed 30 min after the injection (Friedman test, $p \geq 0.05$. n = 29 from 3 mice).

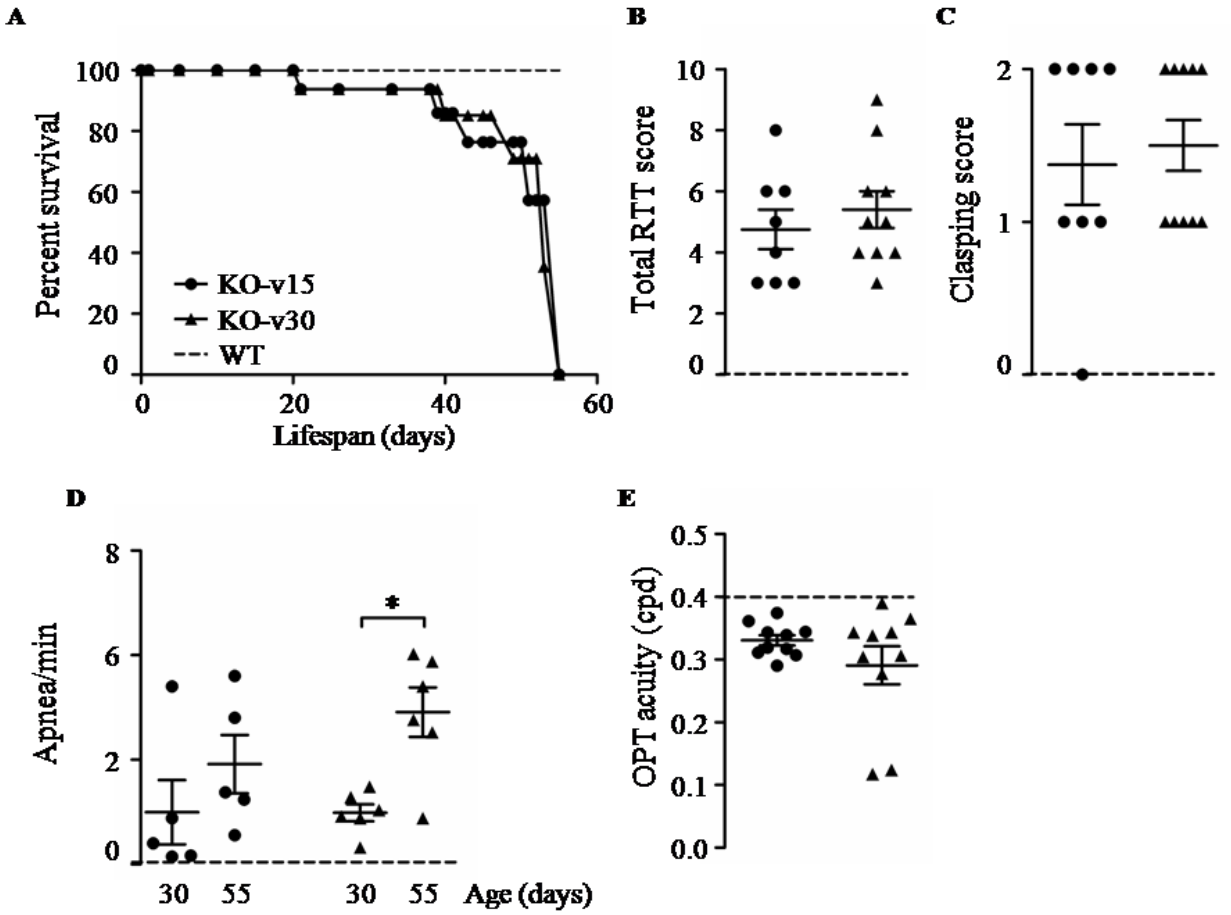

Figure S5. Timing of vehicle treatment does not affect behavioral phenotypes. No differences in the survival rates **(A),** in the overall phenotypic score **(B)** and in the clasping score severity **(C)** between KO-v15 (circle) and KO-v30 (triangle). **(D)** Number of apneas per minute significantly increased developmentally in the KO-v30 but not in the KO-v15 (Wilcoxon signed-rank test, $*p < 0.05$). **(E)** OPT visual acuity did not differ between the two timing paradigms. KO-v15, $n = 8$; KO-v30, $n = 10$. Dotted line represents WT level.

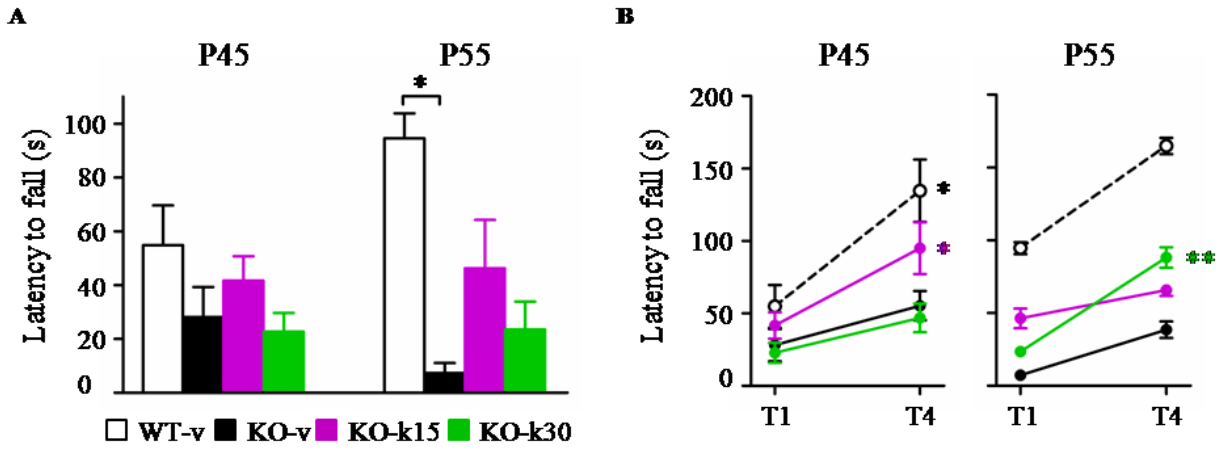

Figure S6. Prolonged ketamine treatment stabilizes motor performance in *Mecp2*-null mice. (A) The latency to fall in KO-v was drastically decreased at P55 compared to WT-v (Kruskal-Wallis, $^{**}p < 0.01$, Dunn's post-test). Neither ketamine treatments fully restored the motor performance of the *Mecp2*-null mice to WT level, but they did not deteriorate with age like the KO-v. **(B)** WT-v mice improved their motor performance at both P45 and P55, over subsequent trials. Despite the lower overall performance, KO-k15 significantly improved at P45 but not at P55. In the same way, KO-k30 improved their performance at P55 but not at P45 (two-way ANOVA, $^{*}p < 0.05$, $^{**}p < 0.01$, Bonferroni post-test. WT-v, $n = 6$; KO-v, $n = 8$; KO-k15, $n = 9$; KO-k30, $n = 11$ mice). Data are expressed as mean ± SEM.

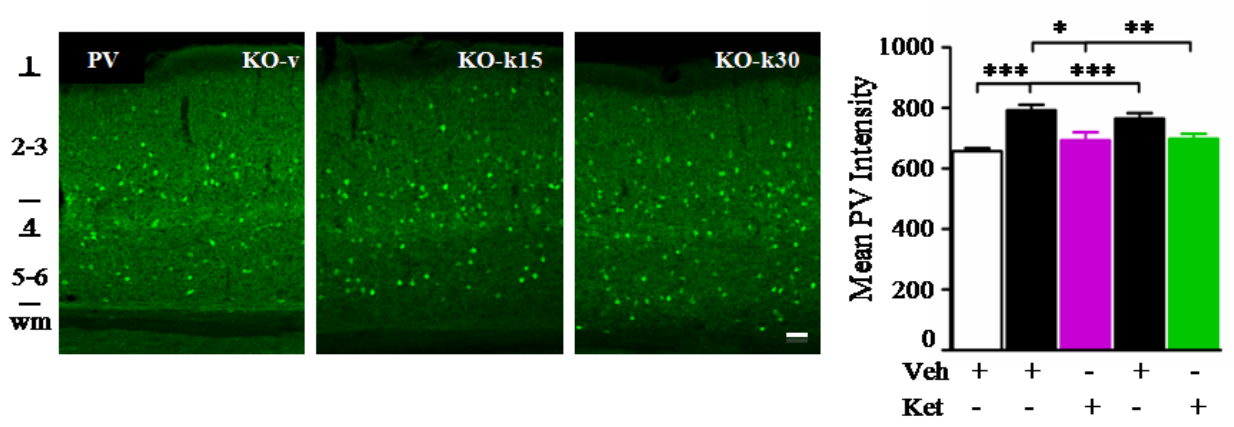

Figure S7. Prolonged ketamine treatment normalizes parvalbumin intensity in the visual cortex of *Mecp2*-null mice. Mean pixel intensity of PV (green) immunofluorescence is increased in KO-v compared to WT-v mice. Both ketamine treatments significantly restored the PV intensity to WT level. (Kruskal-Wallis, *$p < 0.05$, **$p < 0.01$ ***$p < 0.001$, Dunn's post-test. WT-v15, $n = 3$; KO-v15, $n = 3$; KO-k15, $n = 4$; WT-v30, $n = 3$; KO-v30, $n = 4$; KO-k30, $n = 4$ mice). Scale bar 10 m. Data are expressed as mean ± SEM.

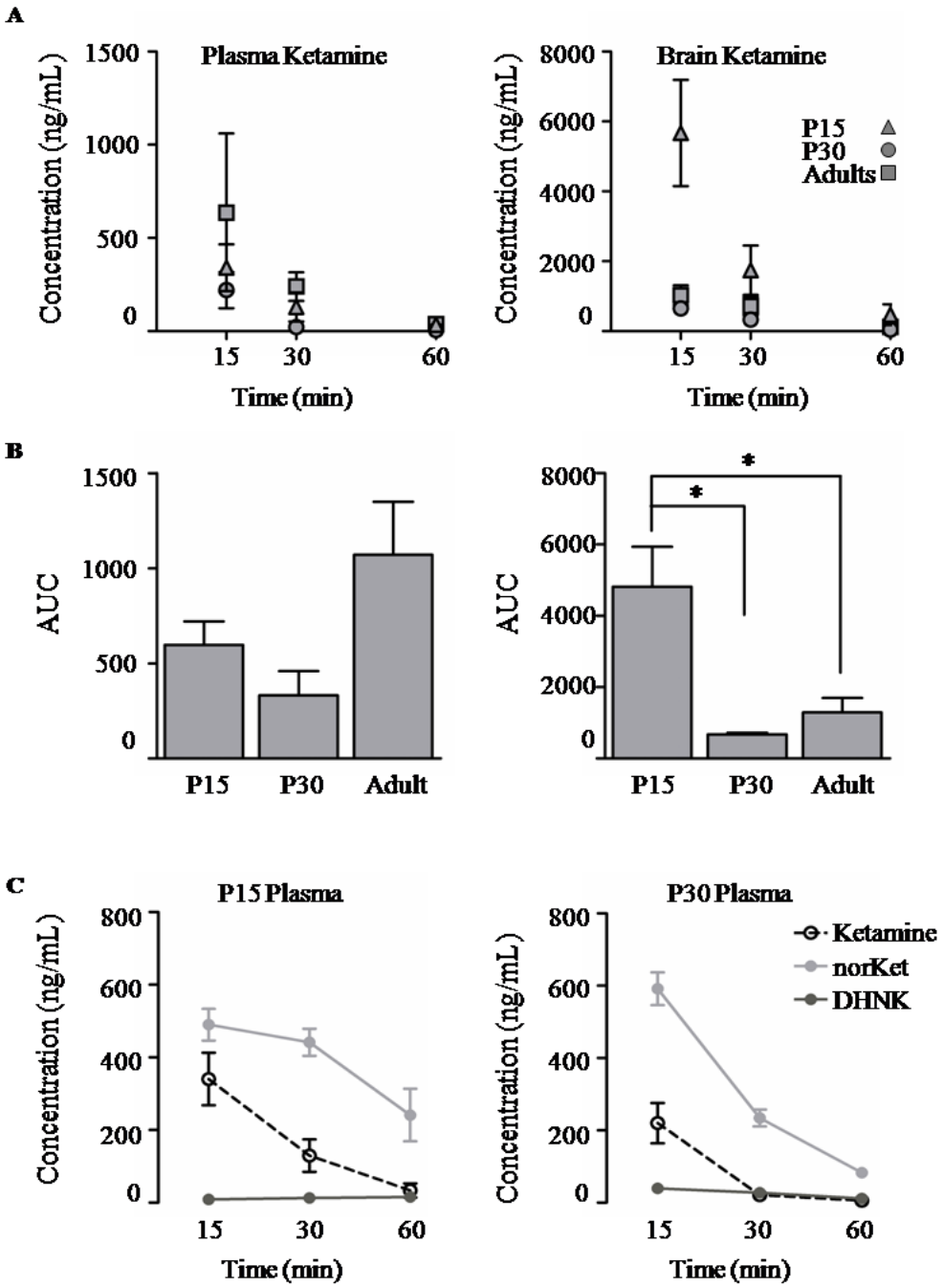

Figure S8. Pharmacokinetic analysis of ketamine 8 mg/kg at different ages. (A) Total ketamine concentration in plasma (left) showed that there were no differences between the two ages indicating similar absorption from the peritoneal cavity. On the contrary, the brain concentration (right) was higher in P15 compared to P30 and adults mice (P15: triangle; P30: circle; Adults: square; n = 3 mice per time point). **(B)** Area under the curve (AUC) for plasma and brain ketamine concentration. (One-way ANOVA, *p < 0.05, Tukey's post-test). **(C)** Ketamine 8 mg/kg was predominantly metabolized in norketamine (norKet) and not dehydronorketamine (DHNK) both at P15 and P30. Data are expressed as mean ± SEM.

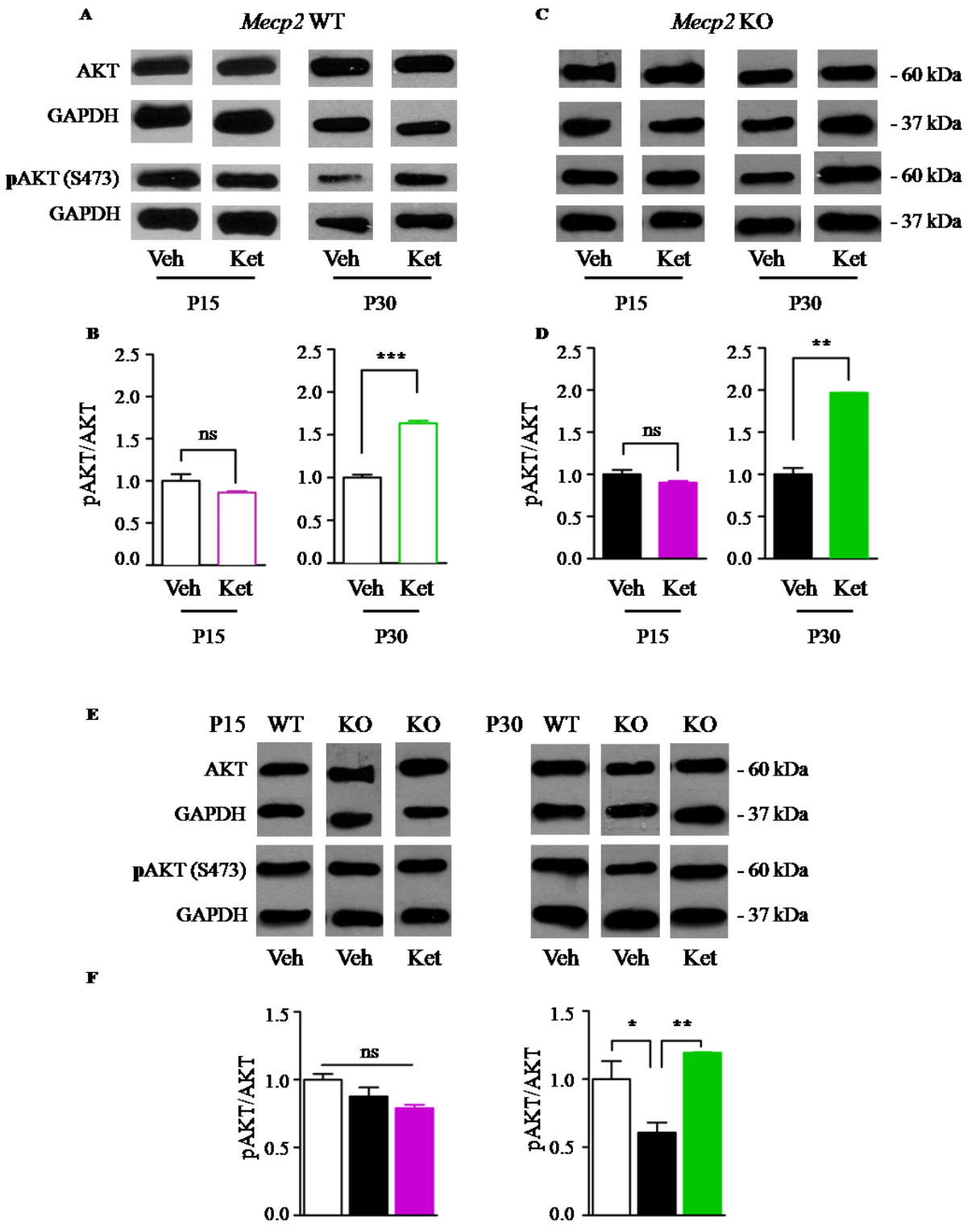

Figure S9. At P30, acute ketamine (8 mg/kg) administration increases AKT phosphorylation (S473) level. (A) Representative Western blots (WB) of AKT and pAKT levels in P15 and P30 *Mecp2* WT mice treated acutely with 8 mg/kg ketamine or vehicle. **(B)** At P30, pAKT/AKT ratio was significantly increased after ketamine treatment compared to vehicle

controls (Student's *t*-test, ***$p < 0.001$). This increase was not seen at P15. **(C)** Representative WB of AKT and pAKT levels in ketamine and vehicle treated *Mecp2* KO mice at P15 and P30. **(D)** As in WT mice, pAKT/AKT ratio was increased at P30 but not at P15 after ketamine treatment (Student's *t*-test, ***$p < 0.001$). **(E)** Representative WB of AKT and pAKT levels in P15 and P30 *Mecp2* WT and KO mice acutely treated with 8 mg/kg ketamine or vehicle. **(F)** pAKT/AKT ratio was significantly decreased in *Mecp2* KO mice at P30, but not at P15, as compared to age-matched WT controls. Acute ketamine administration restored pAKT/AKT ratio in *Mecp2* KO at P30 (one-way ANOVA,*$p < 0.05$; **$p < 0.01$, Holm-Šidák post-test). (n = 3 per each treatment and genotype). Data are expressed as mean ± SEM.

Table S1. Prolonged ketamine treatment does not rescue gross morphological phenotypes.

Genotype and Treatment	PV-cell Density (mm^2)	Thickness (mm)	NeuN Soma Size (mm^3)
WT-v	1.3 ± 0.02	834.4 ± 11.04	590.4 ± 11.63
KO-v	1.4 ± 0.02	721.1 ± 7.44***	495.9 ± 13.37**
KO-k15	1.5 ± 0.1	699.7 ± 9.77***	492.5 ± 23.61*
KO-k30	1.4 ± 0.04	703.6 ± 10.30***	505.4 ± 25.03*

One-way ANOVA, *$p < 0.05$, **$p < 0.01$, ***$p < 0.001$, Bonferroni post-test.

Supplementary Methods and Materials

Animals

Mecp2 animal stock was maintained on a C57BL/6J background. Experimental *Mecp2* mice were in a F1 isogenic strain background generated by mating *Mecp2*-heterozygous (Het) females to C57BL/6J (Jackson Laboratories) male mice (1). GluN2A KO mice (M. Mishina, University of Tokyo) (2) derived from multiple backcrossing onto a C57BL/6J background. All experiments were performed with littermate and age-matched wild-type animals as controls. Mice were kept with littermates and maintained on a 12-h light/ dark cycle and provided with food and water *ad libitum*.

Drug Treatment

A subset of *Mecp2* wild-type (WT) mice received a single acute injection to perform pharmacokinetic analysis and behavioral assays (locomotor activity and pre-pulse inhibition). A second set of *Mecp2* WT and *Mecp2*-null mice were injected daily starting from postnatal day 15 (P15) or P30 for 40 days or 25 consecutive days, respectively. All animals from this second cohort were first tested behaviorally as for the first set, then used for *in vivo* single unit recordings, and finally perfused for immunohistochemistry.

Pharmacokinetic Analysis

P15 and P30 mice were euthanized in a CO_2 chamber at 15, 30, 60 minutes after dosing. Adult mice were euthanized in a CO_2 chamber at 5, 15, 30, 60, 120 minutes after dosing. Whole blood was collected by cardiac puncture into Vacutainer tubes containing EDTA and stored on ice until centrifuged for the separation of plasma. Whole brains were collected by decapitation, rinsed

with PBS, and immediately frozen on dry ice upon collection. The concentrations of ketamine in brain and plasma samples were determined by liquid chromatography with mass spectrometry detection (LC/MS model 6410QqQ, Agilent Co.). Raw samples were pre-processed to precipitate proteins, solubilize the drug and add deuterated ketamine as the internal standard. The analytical method was developed and validated using freshly made calibrators and spiked bank samples. Following an initial non-compartmental analysis, the pharmacokinetics of ketamine were characterized with a two compartment model assigning the brain concentrations to the peripheral compartment. The best parameter estimation was achieved by fitting simultaneously plasma and brain data, using goodness-of-fit, residuals and information criteria (Phoenix, Pharsight Co.) (3). The area under the curve was calculated using GraphPad Prism (version 5.0) software.

Neurobehavioral Characterization

Spontaneous Locomotor Activity. Activity was measured using photo beam breaks in a 30 min session in two Plexiglas transparent open fields (25 cm long, 25cm wide, 20 cm high), each with 2 infra-red frames using ActiTrack software (Panlab/Harvard Apparatus).

Phenotypic Scoring. Mice were scored from 0–2 for 6 parameters including mobility, gait, hind-limb clasping, breathing, tremor and general condition. A score of 0 represents the absence of symptoms, 1 indicates the symptom is present, and 2 indicates the symptom is very severe.

Rotarod. Mice were habituated to the rod for one day prior to the test. The second day each mouse was given four trials on the apparatus. The latency time was recorded for each consequential trial. Between each trial the mouse was placed back in its cage for a minimum of 5 minutes to recover from physical fatigue.

Prepulse Inhibition of the Startle Reflex. Prepulse inhibition (PPI) of the acoustic startle response was conducted using the Startle Monitor (Kinder Scientific). Thirty minutes after vehicle or ketamine (8 or 56 mg/kg, i.p.) mice were placed in a small-sized, nonrestrictive, cubical Plexiglas recording chamber (27 cm × 10 cm × 12.5 cm) fixed on a piezo/plexiglass sensing assembly and allowed to acclimate for 5 min with a 60 dB background white noise. This noise continued throughout the entire session which consisted of 4 testing blocks. In the first testing block, the initial startle response amplitude was determined by delivering a 40 ms pulse of 105 dB broadband white noise. In the second and third testing blocks, the mice were exposed to a series of “pulse-only” or “prepulse-pulse” paired stimuli. The pulse-only stimulus consisted of a 40 ms stimulus of 105 dB. The prepulse-pulse paired trials were conducted by delivering a single 20 ms prepulse, with an intensity of 74, 78 or 82 dB 100 ms before a 40 ms stimulus with an intensity of 105 dB. Each prepulse-pulse paired trial was repeated 5 times, pulse only trials were repeated 5 times in a pseudorandom order, with 30 s average (range 25 - 35 s) inter-trial interval. The recording window for a startle response was 250 ms after the 105 dB startle pulse.

Optomotor Task. Visual threshold acuity was evaluated using published methods (4). In brief, vertical sine wave gratings were projected as a virtual cylinder in three-dimensional coordinate space on four computer monitors arranged in a quadrangle around a testing arena (OptoMotry; CerebralMechanics). Unrestrained animals were placed on an elevated platform at the epicenter of the arena. The experimenter followed the mouse’s head with a crosshair superimposed on the video image to center the rotation of the cylinder at the mouse’s viewing position, thereby clamping the spatial frequency of the grating. If the mouse’s head tracked the cylinder rotation, it was judged that the animal could see the grating.

A process of incrementally changing the spatial frequency of the test grating was repeated until the highest spatial frequency tracked was identified as the threshold. A threshold for each direction of rotation was assessed and the highest spatial frequency tracked in either direction was recorded as the visual acuity. Each session lasted generally 15-20 minutes per mouse. To evaluate the development of visual acuity, mice were tested every 3-5 days starting after eye opening until P60. Experimenters were blind to genotype and the animal's previously recorded thresholds. All animals were habituated before the onset of testing by gentle handling and placing them on the arena platform for a few minutes at a time the same day of testing.

In Vivo Single Unit Recordings

In vivo recordings were performed at adulthood (P55-60), under Nembutal (50 mg/kg, i.p.) / chlorprothixene (0.025 mg/kg, i.m.) anesthesia using standard techniques (5; 6). For each mouse, 2 to 4 penetrations were performed across the medio-lateral extent of binocular V1. Responses were recorded using multichannel probes (A1 x 16-3 mm 50 -177, Neuronexus Technologies) and the signal was amplified, thresholded and discriminated (SortClient, Plexon Technologies). Full-screen sine wave gratings (100% contrast, 0.025 cpd, 2 Hz) were presented on a screen (mean luminance = 32 cd/m^2). Orientations varying between 0 – 360° (12 steps - 30° spacing) were presented in random order (3 sec each - 8 repeats). A uniform gray screen of intermediate luminance was used to monitor spontaneous activity (3 sec - 8 repeats).

Based on their waveforms (7), we selected and analyzed only excitatory cells. Single-unit isolation was ensured by analyzing the cell waveforms and discriminated on the basis of their individual characteristics (Offline Sorter, Plexon Technologies). Activity analysis was done

using MATLAB via SigTOOL (8). Coefficient of variation, measuring the response variability to the preferred gratings, was calculated according to a previous study (9).

Criteria were imposed on the orientation tuning curves to exclude neurons with weak visual responses. Only cells with a maximal-evoked-response > 0.3 spike / sec were kept in the analysis.

Immunohistochemistry

Vehicle and treated mice were transcardially perfused with 4% paraformaldehyde. Brains were extracted, post-fixed in the same fixative, cryoprotected in sucrose and sectioned with a cryostat. Cryosections were first incubated for 30 minutes at room temperature in blocking solution of 97% StartingBlock Buffer (Thermo Sceintific) and 5% of 20% Triton X-100 (Sigma) in PBS. Immunostaining was performed with the following primary antibodies: rabbit anti-parvalbumin (Swant, 1:1000 dilution), guinea pig anti-parvalbumin (Frontiers Institute, 1:1000), mouse anti-GAD65 (Developmental Studies Hybridoma Bank, 1:1000), mouse anti-NeuN (Millipore, 1:1000). The sections were then incubated for 1 hour in secondary antibody at room temperature. The following secondary antibodies were used for fluorescence labelling: Alexa Fluor 488 goat anti-mouse (1:1000), Alexa Fluor 594 goat anti-rabbit (1:500) and Alexa Fluor 594 goat anti-guinea pig (1:500) (Invitrogen). Floating sections were mounted on glass slides and covered with DAPI Fluoromount-G mounting medium (Southern Biotech).

Immunofluorescence and Confocal Microscopy. The sections were analyzed with a laser scanning confocal microscope (Olympus FluoView, FV1000), using the multi-channel acquisition mode to avoid fluorescence cross-talk. Quantitative analyses were performed on a

minimum of three to five mice per genotypes. The binocular zone of visual cortex across all layers was analyzed in 5 to 7 coronal slices.

For parvalbumin expression analysis, 1024 x 1024 fields of primary visual cortex were imaged using a 20x objective (0.75 numerical aperture). The mean pixel intensity of the parvalbumin signal in each field was measured using Fiji software (http://fiji.sc/Fiji).

To analyze parvalbumin-positive presynaptic boutons, images were acquired with a 100x oil-immersion objective (1.4 numerical aperture) and the pinhole set at 1 Airy unit. The number of perisomatic synapses was determined on images triple stained for parvalbumin, GAD65 and DAPI. Presynaptic innervations on pyramidal neurons were analyzed with Fiji software using the analyze particles function and 0.05-10 mm^2 as the initial parameters (10).

To measure NeuN-positive cell density, images (800 x 800 pixels) were acquired with a 60x oil-immersion objective (1.42 numerical aperture) and the pinhole set at 1 Airy unit. Cell density per area was estimated using ImageJ software. After a manual threshold to the single channel we automatically counted total number of cells per each channel. Cell density per volume was calculated with the dissector method (11) applied to z-stacks of confocal sections. Images were processed with the image-analysis program Volocity (5.5; PerkinElmer). We counted all NeuN- and DAPI-positive cells contained within an individual volume but not touching the exclusion sides (top and left side of each optical section). Finally, the number of cells was divided by the volume of the neuropil examined, resulting in cell density.

Western Blot. Visual cortical tissues were extracted from the skull, sonicated, and homogenized in RIPA lysis buffer (20 mM $NaPO_4$ pH 7.4, 10 mM EDTA, 10 mM EGTA, 200 mM NaCl, 20 mM sodium pyrophosphate, 50 mM NaF, 4% Triton X-100, 1% deoxycholate, 2 mM sodium orthovanadate, and a mixture of protease and phosphatase inhibitors from Sigma-Aldrich) at

4°C. Lysates were clarified by centrifugation for 15 minutes at 21,000*g*, and protein concentration of the supernatant was determined using a Bradford reagent assay. Lysates were boiled in SDS sample buffer, separated by SDS-PAGE and blotted to a nitrocellulose membrane (Whatman Protran). The membrane was blocked with 5% milk in Tris-buffered saline Tween-20 (TBST) (10 mM Tris–HCl, pH 8.0, 150 mM NaCl and 0.05% Tween-20), and incubated with primary antibodies for 16 hours at 4°C. The following primary antibodies were used: rabbit monoclonal anti-AKT (1:1000, Cell Signaling Technology), rabbit monoclonal anti-phospho AKT (Ser473) (1:2000, Cell Signaling Technology), and mouse monoclonal anti-GAPDH (1:40000, Abcam). After washing three times with TBST, membranes were incubated with peroxidase-conjugated secondary antibodies (anti-mouse (1:5000) or rabbit IgG (1:1000); Abcam). Detection was performed by enhanced chemiluminescence (Amresco). For quantitative measurements, autoradiographs were scanned and signal intensity assessed with ImageJ (NIH) software.

Supplemental References

1. Guy J, Hendrich B, Holmes M, Martin JE, Bird A (2001): A mouse Mecp2-null mutation causes neurological symptoms that mimic Rett syndrome. *Nat Genet*, 27: 322–326.

2. Sakimura K, Kutsuwada T, Ito I, Manabe T, Takayama C, Kushiya E, *et al.* (1995): Reduced hippocampal LTP and spatial learning in mice lacking NMDA receptor epsilon 1 subunit. *Nature*, 373: 151–155.

3. Chenel M, Barbot A, Dupuis A, Mimoz O, Paquereau J, Bouquet S, Couet W (2003): Pharmacokinetic-pharmacodynamic modeling of the electroencephalogram effect of norfloxacin in rats. *Antimicrob Agents Chemother*, 47: 1952–1957.

4. Prusky GT, Alam NM, Beekman S, Douglas RM (2004): Rapid quantification of adult and developing mouse spatial vision using a virtual optomotor system. *Invest Ophthalmol Vis Sci*, 45: 4611–4616.

5. Gordon JA, Stryker MP (1996): Experience-dependent plasticity of binocular responses in the primary visual cortex of the mouse. *J Neurosci*, 16: 3274–3286.

6. Hensch TK, Fagiolini M, Mataga N, Stryker MP, Baekkeskov S, Kash SF (1998): Local GABA circuit control of experience-dependent plasticity in developing visual cortex. *Science*, 282: 1504–1508.

7. Niell CM, Stryker MP (2008): Highly selective receptive fields in mouse visual cortex. *J Neurosci*, 28: 7520–7536.

8. Lidierth M (2009): sigTOOL: A MATLAB-based environment for sharing laboratory-developed software to analyze biological signals. *J Neurosci Methods*, 178: 188–196.

9. Picard N, Leslie JH, Trowbridge SK, Subramanian J, Nedivi E, Fagiolini M (2014): Aberrant Development and Plasticity of Excitatory Visual Cortical Networks in the Absence of cpg15. *J Neurosci*, 34: 3517–3522.

10. Durand S, Patrizi A, Quast KB, Hachigian L, Pavlyuk R, Saxena A, *et al.* (2012): NMDA receptor regulation prevents regression of visual cortical function in the absence of Mecp2. *Neuron*, 76: 1078–1090.

11. Howard CV, Reed MG (2005): *Unbiased Stereology: Three-Dimensional Measurement in Microscopy, 2nd ed.* Taylor & Francis Group.